Results in Physics 7 (2017) 2302–2310

Contents lists available at ScienceDirect

Results in Physics

journal homepage: www.journals.elsevier.com/results-in-physics

Sb_2Te_3 crystal a potential absorber material for broadband photodetector: A first-principles study

Abdullahi Lawal [a,b,*], A. Shaari [a], R. Ahmed [a], Norshila Jarkoni [a]

[a] Department of Physics, Faculty of Science, Universiti Teknologi Malaysia, 81310 Skudai, Johor, Malaysia
[b] Department of Physics, Federal College of Education, Zaria, Nigeria

ARTICLE INFO

Article history:
Received 6 February 2017
Received in revised form 6 April 2017
Accepted 23 June 2017
Available online 30 June 2017

Keywords:
DFT
Quasi-particle many-body perturbation theory
Bethe-Salpeter equation
Second generation TIs
Electron-hole interaction

ABSTRACT

Antimony telluride (Sb_2Te_3), a layered semiconductor material, is considered a promising absorbing material for a high-performance optoelectronic device within broadband wavelengths because of remarkable features like strong optical absorbance and the narrow direct band gap. In this work, based on the first-principles approach, we investigate in detail the structural, electronic and optical properties of the hexagonal Sb_2Te_3 compound. The structural and electronic properties were computed using the first-principles approach, treating exchange–correlation potential with generalized gradient approximation (GGA) within density functional theory (DFT). Furthermore, for accurate prediction of the band gap, we go beyond DFT and calculated band structure using GW correction. The optical properties, namely, imaginary and real parts of complex dielectric function, absorption coefficient, refractive index, reflectivity, extinction coefficient, electron energy loss function and optical conductivity are performed by quasi-particle many-body perturbation theory (MBPT) via Bethe-Salpeter equation (BSE). The computed structural parameters are in good agreement with available experimental data. The obtained quasi-particle (GW) correction band structure show the semiconducting character of Sb_2Te_3 material with a direct band gap E_g of 0.221 eV, in agreement with previously reported value (E_g = 0.210 eV) while the projected density of states indicates (PDOS) that the p-orbital of Sb and Te atoms are responsible for material properties near the Fermi level. To our knowledge, our first reported calculations of optical properties, with the inclusion of electron-hole effects are consistent with available experimental measurements. Consistencies of our findings with experimental data validate the effectiveness of electron-hole interaction for theoretical investigation of optical properties.

Introduction

The rapid demand of the high-performance photo-detector in terms of wavelength and efficiency is increasing day by day due to its versatility of the applications in our daily lives such as biomedical imaging, quantum computing, gas sensing, optical communication, homeland security, remote sensing high-speed optoelectronic and laser photonics [1,2]. In this regard, nowadays, second generation topological insulators (TIs) mainly Sb_2Te_3, Bi_2Te_3 and Bi_2Se_3 have received great attention as an appealing materials for optoelectronic and photonic applications within wide energy spectrum (ultraviolet, visible and infrared spectra), because they have several merits compared with other materials such as narrow band gap, protected conducting surface edges states, saturable absorber character, very high damage threshold, low saturable optical intensity, easily synthesize and low cost [3]. Although these small band gap semiconductors are typically reported the excellent candidates for thermoelectric applications [4], recently their investigations for the optoelectronic applications have shown them suitable for optoelectronics as well. Due to its time-reversal symmetry and strong spin–orbit coupling (SOC) effect, Sb_2Te_3 has reported a topological insulator with protected gapless surface states which makes it different from the other conventional semiconductors [5,6]. It has also, recently, gained special attention as a promising absorbing material in optoelectronic devices due to its direct band gap, strong optical absorbance, and formation of single massless Dirac cone at the surface [7]. Therefore, in order to understand the optoelectronic nature of Sb_2Te_3 and its scope for futuristic applications, a detailed knowledge of electronic structure and optical properties is essential.it is known that Sb_2Te_3 has five atomic layers structure in the primitive cell containing three different atoms classified as Te-1, Te-2 and Sb

* Corresponding author at: Department of Physics, Federal College of Education, Zaria, Nigeria.
E-mail address: abdullahikubau@yahoo.com (A. Lawal).

http://dx.doi.org/10.1016/j.rinp.2017.06.040
2211-3797/

leading to (Te-1)-Sb-(Te-2)-Sb-(Te-1) sequence along *c*-axis with a rhombohedral crystal structure and belongs to $R\bar{3}m(166)$ space group. Alternatively it is described in hexagonal unit cell of 15 atoms similar to graphene along x–y plane with sandwiched layered structure, called quintuple layered forming a slab of five atomic layers. The quintuple layers (QLs) are stacked along *c* axis direction held together by weak van der Waals interaction and covalently bonded within the QLs. Theoretical investigations by various *ab initio* methods and experimental studies have shown that Sb_2Te_3 is a narrow-gap semiconductor and the band structure depends on spin–orbit interaction [5,8]. Although extensive calculations have been conducted on electronic structure of Sb_2Te_3 [9] using first-principles approach, most of the electronic structure calculations are performed based on generalized gradient (GGA) or local-density (LDA) approximations.

The quality of the DFT calculations considerably depends upon the suitable choice of the exchange–correlation approximation. Nevertheless, GGA and LDA functional based calculations concerning surface states show good agreement with the experimental results [10], they usually demonstrate inappropriate values of the electronic band gap, particularly for semiconductors and insulators. It is because the quasiparticle (QP) band structure is not predicted well by the Kohn-Sham eigenenergy values. In order to overcome this discrepancy between DFT calculations at the level of GGA/LDA and the experimental results, self-energy corrections to the QP energy GW are needed [11].

Optical parameters, namely imaginary and real parts of complex dielectric function, electron energy loss function, absorption index, refractive index, reflectivity, extinction coefficient and optical conductivity are used to characterize the optoelectronic behaviour of any condensed-matter systems for technical application. Therefore, it is essential to be able to accurately describe such quantities with an efficient and reliable approach that provide a satisfactory description in agreement with experimental findings. Optical properties of Sb_2Te_3 have been extensively studied experimentally [12–20], compared to theoretical study. For quite decades, optical properties of the materials have been investigated extensively with standard DFT using independent particle approach of Ehenreich and Cohen [21,22] and one-particle Green's function approach within GW approximation [23]. However, neither of these methods provides a correct evaluation of optical spectra, because the optical spectrum and the shape of the calculated dielectric function show significant differences from those obtained in experimental measurement [24–27]. The limitation of standard DFT and one-particle Green's function is their failure to describe the excitonic effect of electron-hole interaction which requires two-particle approach. It has been known that two-particle approach provides a correct description of optical properties of a number of systems due to the influence of electron-hole correction in optical spectra. Several *ab initio* calculations of the optical spectra, within the inclusion of electron-hole interaction using different approximations and techniques for different materials like Li_2O, TiO_2, and polythiophene, have shown their reliability and agreement with experimental data [26,28,29]. Therefore, for effective description of optical spectra, the excitonic effect due to electron-hole interaction should be included. Moreover, to the best of our knowledge, *ab initio* calculations of optical properties with the inclusion of electron-hole effects for Sb_2Te_3 have not been reported yet. Therefore, our main motivation here is to calculate structural, electronic and optical properties of Sb_2Te_3 within the inclusion of electron-hole effects and compare them with the standard DFT results and experimental measurements.

In this paper, electronic properties of Bi_2Te_3 in the hexagonal structure are calculated using Green function and screened Coulomb interaction (GW) method and are compared with the standard DFT calculated band gap results. For optical properties, we employed a technique that introduced electron-hole interaction into first-principles many-body perturbation theory (MBPT) via Bethe-Salpeter equation (BSE) approach as implemented in YAMBO package.

Theoretical methodology

Theoretically, Schrödinger equation (SE) is a quantum mechanical expression that provides an exact description of system's physical properties such as particle motion and its wave function. The electronic structures of any system can be accurately obtained via the solution of SE without any semi-empirical or empirical parameters [30,31]. However, SE is difficult to solve due to electron-nucleus interaction, then later a solution was proposed by famous Born-Oppenheimer approximation. Previous researchers think that to separate nuclear coordinates and electronic from many-body wave function, the nuclei should be treated adiabatically because of differences in mass between nuclei and electron [32]. Despite with this simplification still, many-body problem remain difficult. Then with Hartree-Fock (HF) approximation problem of many-electron can be simplified to single electron and provide a correct description of electron exchange, unfortunately, it failed to describe electronic correlation [33]. As it is not possible to solve SE directly for N-electron, then in 1964 density functional theory (DFT) was proposed by famous Hohenberg and Kohn as a method to determine the electronic structure of a system at ground state with a theory stated that all ground state properties for many particle systems are functional of the electron density [34,35]. The minimum value of the total energy functional is the ground state energy and this energy is the exact single electron ground state density [36]. Kohn and Sham proposed an equation that replaced the problem of mutually interacting electrons in an external ion potential to an equivalent set of self-consistent one-electron [37]. The effects of electron–electron interactions are expressed by generalized gradient approximation (GGA) [38] or local density approximation (LDA) [39]. Calculations based on DFT are distinguished from other *ab initio* approaches as first-principles calculation with an approximate error of 10^{-3} eV, the errors can be minimized by adjusting the cut-off energy or k-points mesh. In many cases, the first-principles approach within the framework of DFT gives accurate predictions of various properties of materials, stable configuration and total energy.

In this paper, geometry relaxation and electronic properties of Sb_2Te_3 were performed by the first-principles approach based on plane-wave self-consistent field (PWSCF) program within the framework of DFT as implemented in Quantum-Espresso simulation package [40]. Full relativistic norm-conserving pseudopotentials of the standard solid state pseudopotential library of Dal Corso et al. [41,42] were used to model the interaction between valence electron and ionic core potential for Sb, Te-1, and Te-2 with and without the inclusion of spin–orbit coupling (SOC). A generalized gradient approximation (GGA) of Perdew–Berke–Erzndof (PBE) is used in order to treat electron–electron interaction [38]. Plane waves with kinetic energy cutoffs of 30 Ry were used to expand the electronic wavefunctions and 320 Ry for charge density. The irreducible Brillouin zone of electronic structure calculations was sampled with a set of (12 12 12) Monkhorst-Pack grid to generate k-points while denser values of (14 14 14) were used for the density of states using first-order Hermite-Gaussian smearing technique. The initial structure obtained from materials project of Jain et al. [43] were geometrically relaxed for atomic coordinates and dimension of the cell using intrinsic Broyden–Fletcher–Goldfarb–Shanno (BFGS) algorithm [44,45], until atomic maximum forces were less than 5×10^{-5} eV/Å) and the total energy during

iterative process was changing by less than 0.0001 Ry. However, for electronic band structure correction obtained from standard DFT approach, we performed GW calculations within G_0W_0 approximation as implemented in YAMBO package [46] to obtain a real quasiparticle (QP) energies E_n^{QP} correction to the Kohn-Sham eigenvalues E_n^{GGA} as shown in Eq. (1).

$$E_n^{QP} = Z_n\langle\varphi_n^{GGA}|\Sigma_{GW}(E_n^{GGA}) - V_{XC}|\varphi_n^{GGA}\rangle + E_j^{GGA} \quad (1)$$

where Σ_{GW} is the GW self-energy which is the product of one-electron Green's function G and screened Coulomb potential W as iG_0W_0, E_n^{GGA} and φ_n^{GGA} are the KS eigenfunctions and eigenvalues V_{XC} is the DFT exchange–correlation potentials and index n runs over occupied and unoccupied states and Z_n is the orbital renormalization factor which defined as

$$Z_n = \left[1 - \frac{\partial\left\langle\varphi_n^{GGA}|\Sigma_{GW}(E_n^{GGA})|\varphi_n^{GGA}\right\rangle}{\partial E_n^{GGA}}\right]^{-1} \quad (2)$$

The Brillouin zone of GW calculation was sampled with a set of (6 6 6) k-points to ensure convergence of QP energies. The screenings in Coulomb potential W were treated via plasmon-pole approximation. In GW self-energy exchange–correlation part, we used plane-waves kinetic energy cutoff of 20 R. The QP energies values have been converged with the number of empty bands more than 3000. For optical properties calculations, we adopted an approach that provides a correct description of optical spectra in better agreement with experimental data [47], via the solution of two-particle BSE based on GW corrected energies as implemented in YAMBO simulation package [44,46]. The approach involved three stages; the eigenvalue of Kohn-Sham matrix from ground states DFT calculation follow by GW calculation to correct the KS eigenvalue and lastly the solution of BSE using GW eigenvalue to include electron-hole interaction as can be seen in Eq. (3) [25,46].

$$\Omega^s A^s_{vck} = (E_{ck} - E_{vk})A^s_{kvc} + \sum_{k'v'c'}\langle vck|K^i + 2K^r|v'c'k'\rangle \quad (3)$$

where A^s_{vck} and Ω^s are the excited eigenvectors sand eigenvalues, E_{vk} and E_{ck} are the QP energies for the valence and conduction band states, K^r and K^i are the repulsive and interactive exchange terms of electron-hole interaction, c and v are the conduction band, valence band and k wave vector respectively.

The calculation of optical absorption spectra is based on 60 conduction bands and 50 valence bands. The imaginary part of dielectric function $\varepsilon_2(\omega)$ was obtained by direct electronic transitions between occupied (electrons) and unoccupied (holes) electronic states and calculated from Eq. (4) [25], while Kramers-Kronig relations was used for calculating real part of frequency dependent dielectric function as shown in Eq. (5) [48].

$$\varepsilon_2(\omega) = \frac{16\pi e^2}{\omega^2}\sum_S |\vec{\lambda}.\langle O|vec\upsilon|S\rangle|^2\delta(\omega - \Omega^s) \quad (4)$$

$$\varepsilon_1(\omega) = 1 + \frac{2P}{\pi}\int_0^\infty \frac{\omega'\varepsilon_2(\omega')}{\omega'^2 - \omega^2}d\omega' \quad (5)$$

where $\vec{\lambda}$ is the polarization vector of light. $\langle O|vec\upsilon|S\rangle$ is the optical transition matrix from valence to conduction states and P is the principal value of the integral and the integral is over irreducible Brillouin zone.

The knowledge of real and imaginary parts of frequency dependent dielectric function expressions was used to compute other optical parameters namely, absorption index $\alpha(\omega)$, electron loss function $L(\omega)$, refractive index $n(\omega)$, conductivity $\sigma(\omega)$ extinction index $k(\omega)$ and reflectivity $R(\omega)$ as can be seen in the following equations [49,50]:

$$\alpha(\omega) = \frac{\omega}{c}\sqrt{2(\sqrt{\varepsilon_1^2(\omega) + \varepsilon_2^2(\omega)} - \varepsilon_1(\omega))} \quad (6)$$

$$n(\omega) = \sqrt{\left(\frac{\varepsilon_1(\omega) + \sqrt{\varepsilon_1^2(\omega) + \varepsilon_2^2(\omega)}}{2}\right)} \quad (7)$$

$$k(\omega) = \sqrt{\frac{-\varepsilon_1(\omega) + \sqrt{\varepsilon_1^2(\omega) + \varepsilon_2^2(\omega)}}{2}} \quad (8)$$

$$R(\omega) = \left|\frac{\sqrt{\varepsilon(\omega)} - 1}{\sqrt{\varepsilon(\omega)} + 1}\right|^2 \quad (9)$$

$$L(\omega) = \frac{\varepsilon_2(\omega)}{\varepsilon_2(\omega)^2 + \varepsilon_1(\omega)^2} \quad (10)$$

$$\sigma(\omega) = \frac{\omega\varepsilon_2(\omega)}{4\pi} \quad (11)$$

Results and discussion

Structural properties

The primitive cell of Sb_2Te_3 is rhombohedral structure and its conventional cell is hexagonal crystal structure similar to graphene. The geometrical relaxations of Sb_2Te_3 in hexagonal crystal structure were performed to avoid an error for accurate analysis of other properties, such as band structure within the framework of DFT calculations. The theoretical equilibrium lattice parameters $a = b$ and c within LDA, LDA + SOC, PBE and PBE + SOC, together with other previous first-principles calculations and experimental values are shown in Table 1. Clearly, we noted that LDA or LDA + SOC underestimate lattice parameter on c by 3.2%. However, PBE + SOC overestimate c with 6.371% and a by 4.338%. Interestingly, PBE without inclusion of SOC gives lattice constants almost identical with experimental value with only 0.033% error. Therefore, our first-principles calculations suggest that SOC effect on structural relaxation is not important for predicting lattice parameters in the case of second generation topological insulators. We found that PBE exchange correlation potential gives the best match with experimental results when compared with previous theoretical investigations done with other potentials (Fig. 1).

Electronic properties

Electronic band structure calculation is very important for describing the optoelectronic behaviour of materials. Here we perform an analysis of band structure, the total density of state (TDOS) and partial density of state (PDOS) of Sb_2Te_3. The electronic band structures of Sb_2Te_3 were computed within PBE approximation based on DFT and GW self-energy corrections via G_0W_0 approximation along special symmetry directions of the irreducible Brillouin zone setting Fermi energy level scale at 0 eV represented by a red dash as can be seen in Fig. 2a and b respectively. From our band structure calculations with and without inclusion of SOC, the differences in energy between bottom of conduction band and top of valence band are found to occurred at Γ point indicating that Sb_2Te_3 is a direct band gap semiconductor compound having energy at $\Gamma \rightarrow \Gamma$ of 0.120 eV with inclusion of SOC and 0.150 eV in the absence of SOC and these values agreed with previous DFT reports as well [51,56–58]. Table 2 present a summary of our band structure results and available theoretical and experimental mea-

Table 1
Calculated lattice parameter of Sb_2Te_3 compared with previous theoretical and experimental work.

Structure	Work	Method	Lattice parameters		
			a(Å)	c(Å)	c/a
Hexagonal unit cell	Our work	PBE + SOC	4.450	32.390	7.279
		PBE	4.278	30.460	7.120
		LDA + SOC	4.257	29.455	6.919
		LDA	4.243	29.471	6.946
	Previous Work	LDA + SOC [51]	4.252	29.450	6.926
		LDA [51]	4.254	29.460	6.925
		PBE + SOC [52]	4.340	31.359	7.226
		PBE-D2 + SOC [51]	4.248	30.970	7.290
		PBE-D2 [51]	4.246	30.957	7.291
		Exp. [53]	4.271	30.451	7.130
		Exp. [54]	4.264	30.458	7.143
		Exp. [55]	4.265	30.450	7.140

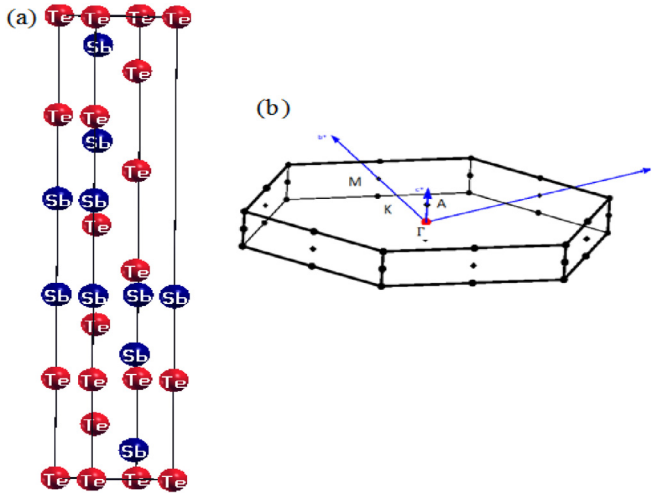

Fig. 1. Structure of Sbi_2Te_3 (a) Bulk Hexagonal unit cell. (b) First Brillouin zone along the high symmetry points.

surements. However, our band gap is smaller than experimental value of 0.150–0.210 eV [12–15], this effect is the limitation of DFT approach due to approximations used for the exchange–correlation functional. We also noticed that hybridization due to SOC lead to the existence of many bands at Γ point in the valence band region with numerous degenerate levels. Next to accurately correct the band gap obtained by standard DFT approach, we introduced a self-energy corrections in the QP energy using MBPT within G_0W_0 approximation. The G_0W_0 approximation confirmed the direct gap of Sb_2Te_3 as reported in transmittance and photoemission spectroscopy measurements. The calculated QP energy gap of 0.221 eV obtained using G_0W_0 approximation agrees very well with transmittance and photoemission spectroscopy. Our calculation pointed out that spin–orbit interaction and GW approximation on top of DFT provide accurate prediction of band structure. Table 2 provides an illustration of the results of our band structure calculations with other previous theoretical and experimental values.

We also have computed and analyzed the total density of states (TDOS) and partial density of states (PDOS) for Sb_2Te_3 as can be seen in Fig. 3(a) and (b) along with the Fermi energy level represented by a red dash. The result of DOS help to elaborate the nature of the band gap and PDOS provides details information about the origin of bands for valence and conduction bands. The s-orbital of Sb, Te-1, Te-2 and p-orbital of Sb contribute to lowest valence band (−13.000 eV to −10.504 eV) while middle of valence band which occurred approximately within (−10.000 eV to −7.000 eV) range is contributed from s-orbitals of Sb, Te-1, Te-2 and p-orbital of Te-1 and Te-2 in which s-orbital of Sb states contributed most. The maximum occupied valence bands (−5.512 eV to ∼0.000 eV) are dominated via s-orbital of Sb and p-orbitals of Sb, Te-1, and Te-2 and it is fundamentally dominated by p-orbitals of Sb and Te atoms. In the unoccupied conduction bands above Fermi level (0.000 eV to 5.000 eV), the p-orbitals of Sb, Te-1, and Te-2 are the main contributors. In general, we noticed that p-orbital of Sb and Te atoms are responsible for material properties near Fermi level. Also based on the analysis above, we observed that in the energy range from −13.000 eV to −7.000 s-orbital of Sb hybridize with s-orbital of Te (Te-1 and Te-2) while p-orbital of Sb strongly hybridize with p-orbitals of Te-1 and Te-2 from −5.512 eV to 0.000 eV. Therefore, these hybridizations confirmed the existence of an interatomic force in Sb_2Te_3 semiconductor material which is also confirmed by Qing et al. [60]. However, the Sb, Te-1 and Te-2 atoms via s-orbital do not play any role in the bonding and transport properties. This shows that our results

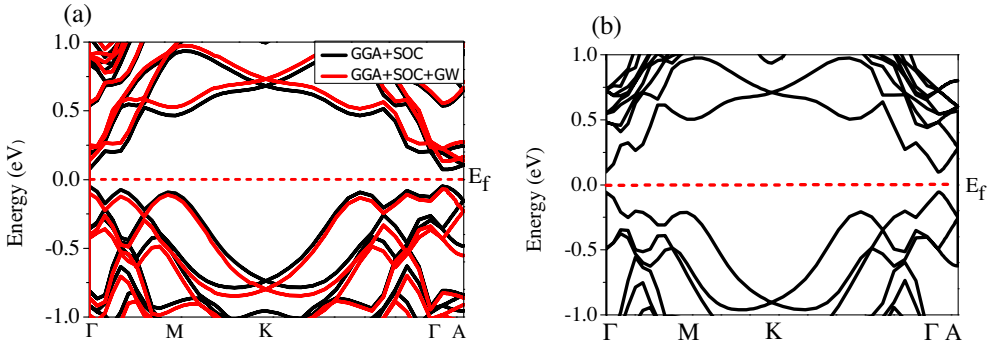

Fig. 2. Band structure of bulk Sb_2Te_3 (a) with and (b) without SOC.

Table 2
Bi_2Te_3 band gap results compared with previous first principle calculations and experimental data.

Work	Methodology	Band gap value Eg (eV)	Type of band gap
Our work	PBE	0.150	Direct
	PBE + SOC	0.120	Direct
	PBE + SOC + GW	0.221	Direct
Previous work	LDA + SOC [51]	0.050	Direct
	DFT-D2 + SOC [51]	0.140	Direct
	PBE + SOC [51,56,57]	0.120	Direct
	Exp. [12–14,59]	0.210	Direct
	Exp. [15]	0.150	Direct

are in good agreement with those from the previous first-principles investigation.

Optical properties

Investigation on the optical properties of materials plays a crucial role in understanding their optoelectronic applications [61]. We have calculated the optical properties by evaluating microscopic dielectric function $\varepsilon(\omega)$ via three different approaches: Random phase approximation (RPA) based on PBE (DFT + RPA) without taking into account the electron–electron and electron-hole interaction, RPA based on G_0W_0 (G_0W_0 + RPA) which neglects electron-hole interaction and solving BSE of many-body perturbation theory (MBPT) based on two interacting QP scheme on top of DFT results to include the role of interaction between the excited electron and hole left in the valence band region (G_0W_0 + BSE). The first Microscopic dielectric function describes the behaviour of linear response of a material to the electromagnetic radiation field applied which displays the absorptive character of that material. Real part of dielectric describes how much material polarized as a result of induced electric dipole creation when electric field is applied while imaginary part indicates how much material absorption photon energy. Fig. 4(a) and (b) present the real and imaginary part of dielectric function of Sb_2Te_3 for polarization along perpendicular direction to the hexagonal axis *c*. Electronic contribution at high frequency and ionic contributions of a non-polar system are contained in the static dielectric permittivity tensor $\varepsilon(0)$ which depends strongly on the material band gap. Static dielectric permittivity tensor and plasma energy can be used to calculate band gap energy E_g via Penn Model expression $E_g \approx \hbar\omega_P/\sqrt{\varepsilon(0)-1}$ [62]. The optical gap in imaginary part of dielectric function represent the inter-band transitions between the conduction band minimum and valence band maximum, which correspond to the fundamental band gap of the material. From optical spectra via DFT + RPA we noticed that the absorption edge, called optical gap is smaller than experimental value, this limitation is due to electronic gap underestimation in DFT. However, inclusion of QP description (G_0W_0 + RPA) shifted the absorption edge to higher energies with respect to DFT + RPA and expected experimental value. Additionally, the optical edges over DFT + RPA and G0W0 + RPA are quite close to electronic gap calculated within PBE and G_0W_0 approximations. The description of optical properties with QP correction and excitonic effects of electron-hole interaction via solution of BSE (G_0W_0 + BSE) gives indeed a definite improvement of results over DFT + RPA and G_0W_0 + RPA as can be seen in Table 3. Comparing the location of fundamental gap edge within G_0W_0 correction and shifted excitonic peak, we deduced an exciton binding energy to be 0.036 eV. This peak is indicated by an arrow in Fig. 4(a). Interestingly, the material can absorb photon energy up to 9.593 eV as the imaginary line approaches zero at that point whereas standard DFT calculations by Park et al. [22] shows that Sb_2Te_3 is transparent above 5 eV which is completely deviated from experimental measurement [19]. The relatively strong absorption in 0.185–9.593 eV energy range provides strong evidence that Sb_2Te_3 has the potential to be used for detecting light within broadband range. Our BSE calculations have almost the same main peaks and amplitude of both real and imaginary part of dielectric function with experimental measurement when compare with the results obtained via standard DFT [22]. These validate the effectiveness of the inclusion of the electron-hole effects for theoretical investigation of optical properties. The dielectric constant at high frequency along perpendicular $\varepsilon_{\perp}(\infty)$ direction was found to be 55.986, 37.542 and 33.804 for DFT + RPA, G_0W_0 + -BSE and G_0W_0 + RPA respectively, showing that the dielectric constant at high frequency obtained via G_0W_0 + BSE is in good agreement with experimental value of 38.000 [16].

The refractive index is a quantity that describes how much light is refracted after entering material [63]. Fig. 5(a) and (b) shows the refractive index $n(\omega)$ and extinction index $k(\omega)$ of Sb_2Te_3 as a func-

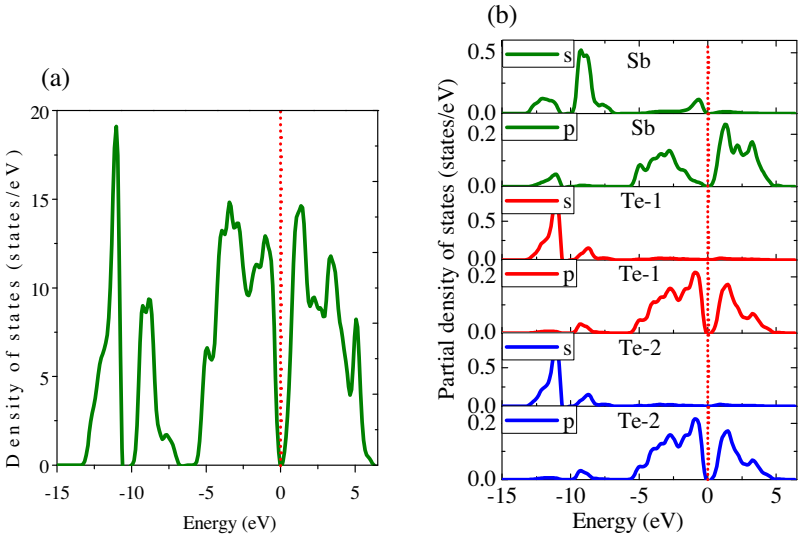

Fig. 3. Density of state (a) Total DOS and (b) Partial DOS for Bi_2Te_3.

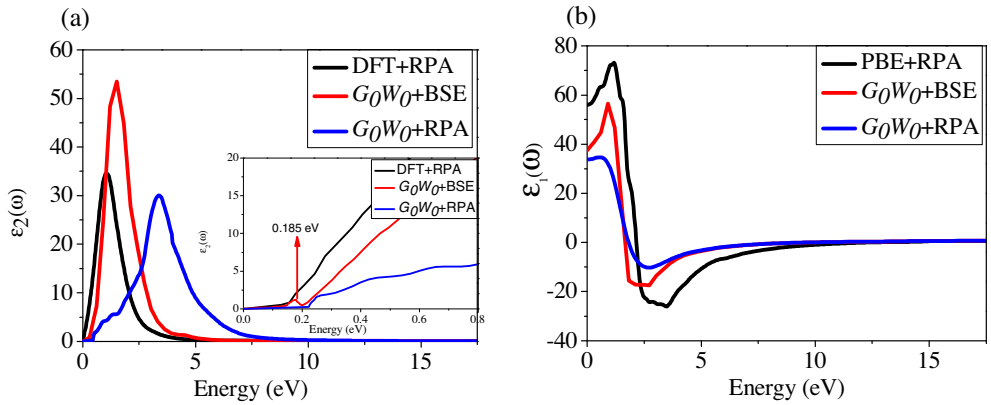

Fig. 4. (a) imaginary part of the dielectric function (b) real part of the dielectric function of Sb_2Te_3 calculated using DFT + RPA, G_0W_0 + RPA, and G_0W_0 + BSE.

Table 3
Sb_2Te_3 BSE results compared with experimental and standard DFT data.

		Optical gap (eV)	$\varepsilon(\infty)$	$n(0)$	Reflectivity first edge (%)	Plasma energy (eV)
Our work	DFT + RPA	0.123	55.635	7.482	58.049	8.668
	G_0W_0 + RPA	0.228	33.804	5.436	47.508	11.635
	G_0W_0 + BSE	0.185	37.542	5.943	50.441	9.593
Previous work	Standard DFT	0.08 [22]	45.36 [22]	–	–	–
	Experimental	0.150–0.210 [12–15,19,20]	38.000 [16] 42.000 [18]	6.200 [16]	52.00 [17]	9.500 [19]

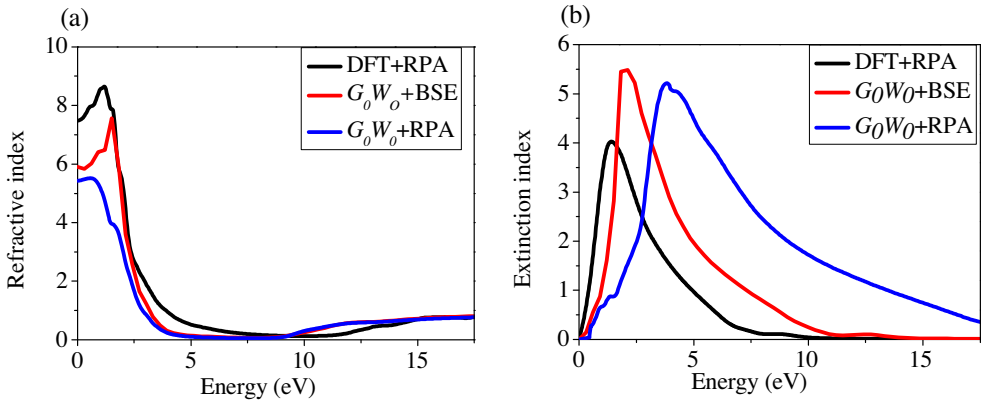

Fig. 5. (a) Refractive index (b) Extinction index calculated using DFT + RPA, G_0W_0 + RPA and G_0W_0 + BSE.

tion of energy at the DFT + RPA, G_0W_0 + RPA and G_0W_0 + BSE level. The static refractive index with inclusion of electron-hole interaction was found to be 5.943, this value is very close to experimental value of 6.200 [16] as listed in Table 3. From the refractive index graph, we noted that the material possesses high refractive index within infrared region around and decreases at higher energy in the visible to UV region. Furthermore, after 3.221 eV the velocity of light is greater than the light celerity because $n(\omega)$ is less than one, this value also is close to spectroscopic ellipsometry measurement [27]. As can be seen in Fig. 5(a), the refractive index with inclusion of electron-hole interaction is smaller than that of DFT + RPA and higher than G_0W_0 + BSE in the whole region from 0 to ~10 eV. These results together with spectroscopic ellipsometry measurement are summarized in Table 3. In the energy range from 0 to 0.185 eV the calculated $k(\omega)$ with inclusion of electron-hole interaction is less than 0.1indicating that Sb_2Te_3 material response to light with wavelength below 6531 nm and then increases rapidly with photon energy forming the maximum peak at 2.136 eV. Our (G_0W_0 + BSE) results of $k(\omega)$ show that Sb_2Te_3 has strong extinction effects within infrared and visible region. On the other hand, the $k(\omega)$ obtained at the DFT + RPA and G_0W_0 + RPA level shows that inclusion of electron–electron interactions shifted the strong extinction effects to UV region. The absorption index is used to describe the extent which a material absorbs photon energy. Fig. 6(a) displays the absorption index of the title material in the three different approaches. It is observed that the absorption spectrum with inclusion of electron-hole interaction begins from 0.185 eV and rises sharply until attaining maximum peak at 12.84×10^7 cm¹ correspond to 2.727 eV and then decreases sharply to 11.932 eV, which reveal the broadband wavelengths absorption behaviour of the title compound. This material shows good absorption coefficient in the region from 1.295 to 7.214 eV. In the absence of electron-hole interaction, the absorption index without (DFT + RPA) and with (G_0W_0 + BSE) inclusion of electron–electron interaction shows prominent peaks at 2.186 and 5.867 eV respectively.

Reflectivity is the ratio of reflected photon energy from surface to the photon energy incident on the surface. Fig. 6(a) displays the

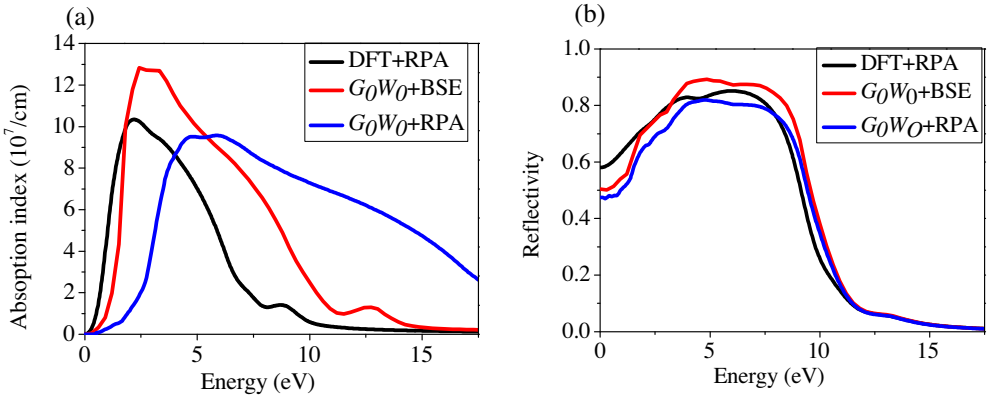

Fig. 6. (a) Absorption index (b) Reflectivity calculated using DFT + RPA, G_0W_0 + RPA, and G_0W_0 + BSE.

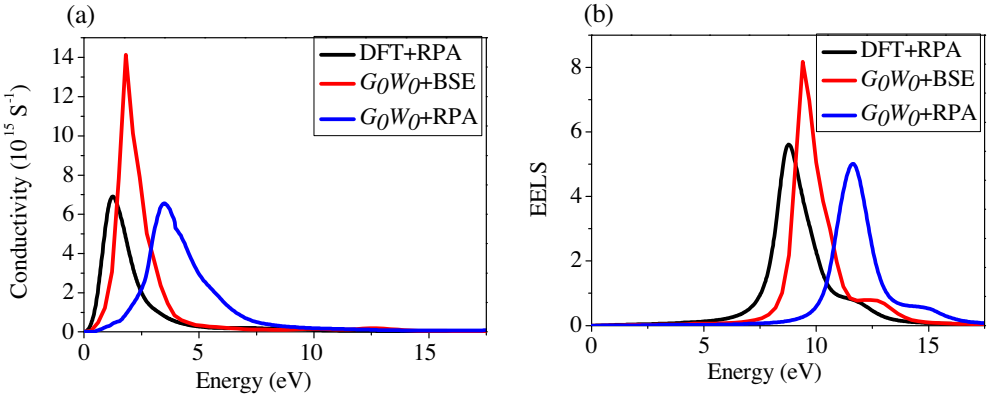

Fig. 7. (a) Conductivity (b) EELS calculated using DFT + RPA, G_0W_0 + RPA, and G_0W_0 + BSE.

changes of reflectivity spectrum with photon energy; the first edge of this parameter with G_0W_0 + BSE was found to be 50.441%, this value is close to available experimental data reported by Langhammer et al. [17]. The reflectivity spectrum starts to increase sharply from 50.441% until attaining maximum level at 89.259% corresponding to photon energy value of 4.848 eV and decreases drastically to a very low value. This indicates that the material is transmitting in ultraviolet wavelengths because of small reflectance within that energy range. Also, the values of reflectivity spectrum at zero energy using DFT + RPA and G0W0 + RPA were 58.049% and 47.508% respectively.

A complex conductivity spectrum is a gauge of photoconductivity that gives clear information on the electrical conductivity of a material. Fig. 7(a) shows the complex conductivity spectrum as a function of photon energy calculated using DFT + RPA (electron-hole and electron–electron attraction neglected), G_0W_0 + RPA (electron-hole attraction neglected and electron–electron attraction included), and G_0W_0 + BSE (electron-hole and electron–electron effects included). It is shown that including electron-hole and electron–electron effects (G_0W_0 + BSE) the maximum peak is located at 2.121 eV correspond to 10.120×10^{15} S^{-1}, indicating high absorption at low energy. Therefore, Sb_2Te_3 second generation TIs is more conductive in the incident photon energy range from 1.213 to 3.204 eV. On the other hand the optical conductivity without (DFT + RPA) and with (G_0W_0 + RPA) electron–electron attractions starts at 0.123 and 0.228 eV respectively. Thus these main edges correspond to DFT and G_0W_0 fundamental band gap since absorption spectra are related to optical conductivity. Electron energy loss function is used to describing the loss in energy of a fast moving electron traversing the material. The corresponding electron energy-loss functions in function of photon energy with the three approaches are shown in Fig. 7(b). The prominent peak was found to be 9.593 eV for G_0W_0 + BSE, this value is consistent with experimental data [18,19]. The sharp maxima peak of the energy loss function spectra indicate the existence of plasma resonance and this appear at a particular incident light frequency which corresponds to the trailing edges in the reflection spectra sometimes called plasma frequency ω_P. At this point of energy, the real part of the dielectric function goes to zero indicating rapid reduction in reflectance. Comparison of energy loss function spectra at DFT + RPA and G0W0 + RPA approaches shows that including electron–electron interaction led to shift in the entire spectra to higher energy as can be seen in Fig. 7(b).

Conclusions

In summary, in this paper, we investigated the structural and electronic properties of Sb_2Te_3 TI using DFT pseudopotential approach within generalized gradient approximation. The structural parameters computed show good agreement with reported experimental data. The band structures within G_0W_0approximation show the small band gap semiconducting behaviour of Sb_2Te_3 in very good agreement with experimental value while the partial density of states indicate that the p-orbitals of Sb and Te atoms are responsible for material properties near Fermi level, in agreement with previous theoretical and experimental measurements. Optical properties are calculated by quasi-particle many-body perturbation theory (MBPT) via Bethe-Salpeter equation (BSE) as implemented in Yambo code. Analysis of optical parameters shows that an excellent agreement with available experimental observa-

tions achieved after adding excitonic effects via G_0W_0 + BSE. Consistencies of our findings with experimental data validate the effectiveness of electron-hole interaction inclusion for theoretical investigation of optical properties.

Acknowledgements

The authors acknowledges FRGS research grant (Vot No.4F915) from ministry of High Education Malaysia, Universiti Teknologi Malaysia (UTM), TETFund through Federal College of Education Zaria, Kaduna, Nigeria and Center for information and Communication Teknologi in University Teknologi Malaysia for financial support, facilities and services of high performance computing on this research work.

References

[1] Sharma A, Bhattacharyya B, Srivastava A, Senguttuvan T, Husale S. High performance broadband photodetector using fabricated nanowires of bismuth selenide. Sci Rep 2016;6.
[2] Koppens F, Mueller T, Avouris P, Ferrari A, Vitiello M, Polini M. Photodetectors based on graphene, other two-dimensional materials and hybrid systems. Nat Nanotechnol 2014;9:780–93.
[3] Lee J, Koo J, Chi C, Lee JH. A harmonically mode-locked femtosecond fiber laser using bulk-structured Bi2Te3 topological insulator. 2015 Conference on Lasers and Electro-Optics (CLEO): IEEE; 2015. p. 1–2.
[4] Cao Y, Zhao X, Zhu T, Zhang X, Tu J. Syntheses and thermoelectric properties of Bi_2Te_3/Sb_2Te_3 bulk nanocomposites with laminated nanostructure. Appl Phys Lett 2008;92:143106.
[5] Hsieh D, Xia Y, Qian D, Wray L, Meier F, Dil J, et al. Observation of time-reversal-protected single-Dirac-cone topological-insulator states in Bi_2Te_3 and Sb_2Te_3. Phys Rev Lett 2009;103:146401.
[6] Lawal A. Density functional theory study of electronic properties of Bi_2Se_3 and Bi_2Te_3. Malay J Fund Appl Sci 2017;12.
[7] Zheng K, Luo L-B, Zhang T-F, Liu Y-H, Yu Y-Q, Lu R, et al. Optoelectronic characteristics of a near infrared light photodetector based on a topological insulator Sb_2Te_3 film. J Mater Chem C 2015;3:9154–60.
[8] Park SH, Chae J, Jeong KS, Kim T-H, Choi H, Cho M-H, et al. Reversible fermi level tuning of a Sb_2Te_3 topological insulator by structural deformation. Nano Lett 2015;15:3820–6.
[9] Sosso G, Caravati S, Bernasconi M. Vibrational properties of crystalline Sb_2Te_3 from first principles. J Phys Condens Matter 2009;21:095410.
[10] Zhang H, Liu C-X, Qi X-L, Dai X, Fang Z, Zhang S-C. Topological insulators in Bi_2Se_3, Bi_2Te_3 and Sb_2Te_3 with a single Dirac cone on the surface. Nat Phys 2009;5:438–42.
[11] Crowley JM, Tahir-Kheli J, Goddard III WA. Accurate ab initio quantum mechanics simulations of Bi_2Se_3 and Bi_2Te_3 topological insulator surfaces. J Phys Chem Lett 2015;6:3792–6.
[12] Nguyen T-A, Backes D, Singh A, Mansell R, Barnes C, Ritchie DA, et al. Topological states and phase transitions in Sb_2Te_3-GeTe multilayers. Sci Rep 2016;6.
[13] Procarione W, Wood C. The optical properties of Sb_2Se_3–Sb_2Te_3. Phys Status Solidi B 1970;42:871–8.
[14] Sehr R, Testardi L. The optical properties of p-type Bi_2Te_3–Sb_2Te_3 alloys between 2–15 microns. J Phys Chem Solids 1962;23:1219–24.
[15] Olson J, Li H, Ju T, Viner J, Taylor P. Optical properties of amorphous GeTe, Sb2Te3, and $Ge_2Sb_2Te_5$: the role of oxygen. J Appl Phys 2006;99:103508.
[16] Kuwahara M, Endo R, Tsutsumi K, Morikasa F, Tsuruoka T, Fukaya T, et al. Approach for measuring complex refractive index of molten Sb_2Te_3 by spectroscopic ellipsometry. Appl Phys Lett 2012;100:101910.
[17] Langhammer H, Stordeur M, Sobotta H, Riede V. Optical and electrical investigations of the anisotropy of Sb_2Te_3 single crystals. Phys Status Solidi B 1982;109:673–81.
[18] Dordevic S, Wolf M, Stojilovic N, Lei H, Petrovic C. Signatures of charge inhomogeneities in the infrared spectra of topological insulators Bi_2Se_3, Bi_2Te_3 and Sb_2Te_3. J Phys Condens Matter 2013;25:075501.
[19] Scrocco M. X-ray and electron-energy-loss spectra of Bi, Sb, Te and Bi_2Te_3, Sb_2Te3 chalcogenides. J Electron Spectrosc Relat Phenom 1990;50:171–84.
[20] Stepanov N, Kalashnikov A, Ulashkevich YV. Plasma screening of the fundamental absorption edge in crystals of Bi_2Te_3-Sb_2Te_3 solid solutions with more than 80 mol% Sb_2Te_3. Opt Spectrosc 2014;117:401–5.
[21] Hedin LS. In: Seitz F, Turnbull D, Ehrenreich H, Lundqvist in solid state physics. Academic Press; 1969.
[22] Park J-W, Eom SH, Lee H, Da Silva JL, Kang Y-S, Lee T-Y, et al. Optical properties of pseudobinary GeTe, $Ge_2Sb_2Te_5$, $GeSb_2Te_4$, $GeSb_4Te_7$, and Sb_2Te_3 from ellipsometry and density functional theory. Phys Rev B 2009;80:115209.
[23] Hedin L. New method for calculating the one-particle Green's function with application to the electron-gas problem. Phys Rev 1965;139:A796.
[24] Rohlfing M, Krüger P, Pollmann J. Quasiparticle band structure of CdS. Phys Rev Lett 1995;75:3489.
[25] Rohlfing M, Louie SG. Electron-hole excitations and optical spectra from first principles. Phys Rev B 2000;62:4927.
[26] Marsili M, Mosconi E, De Angelis F, Umari P. Large scale GW-BSE calculations with N3 scaling: excitonic effects in dye sensitised solar cells. arXiv preprint arXiv:160305427. 2016.
[27] Park J-W, Baek SH, Kang TD, Lee H, Kang Y-S, Lee T-Y, et al. Optical properties of (GeTe, Sb_2Te_3) pseudobinary thin films studied with spectroscopic ellipsometry. Appl Phys Lett 2008;93:1914.
[28] Van der Horst J-W, Bobbert P, Michels M, Brocks G, Kelly P. Ab initio calculation of the electronic and optical excitations in polythiophene: effects of intra-and interchain screening. Phys Rev Lett 1999;83:4413.
[29] Albrecht S, Reining L, Del Sole R, Onida G. Ab initio calculation of excitonic effects in the optical spectra of semiconductors. Phys Rev Lett 1998;80:4510.
[30] Filippov A. Nonlinear nonlocal Schrödinger equation in the context of quantum mechanics. Phys Lett A 1996;215:32–9.
[31] Callaway J, March N. Density functional methods: theory and applications. Solid State Phys 1984;38:135–221.
[32] Kuznetsov AM, Medvedev IG. Does really Born-Oppenheimer approximation break down in charge transfer processes? An exactly solvable model. Chem Phys 2006;324:148–59.
[33] Chaikin PM, Lubensky TC. Principles of condensed matter physics. Cambridge Univ Press; 2000.
[34] Hohenberg P, Kohn W. Density functional theory. Phys Rev B 1964;136:864–76.
[35] Dreizler RM, Gross EK. Density functional theory: an approach to the quantum many-body problem. Springer Science & Business Media; 2012.
[36] Payne MC, Teter MP, Allan DC, Arias T, Joannopoulos J. Iterative minimization techniques for ab initio total-energy calculations: molecular dynamics and conjugate gradients. Rev Modern Phys 1992;64:1045.
[37] Kohn W, Sham LJ. Self-consistent equations including exchange and correlation effects. Phys Rev 1965;140:A1133.
[38] Perdew JP, Burke K, Ernzerhof M. Generalized gradient approximation made simple. Phys Rev Lett 1996;77:3865.
[39] Perdew JP, Zunger A. Self-interaction correction to density-functional approximations for many-electron systems. Phys Rev B 1981;23:5048.
[40] Giannozzi P, Baroni S, Bonini N, Calandra M, Car R, Cavazzoni C, et al. QUANTUM ESPRESSO: a modular and open-source software project for quantum simulations of materials. J Phys Condens Matter 2009;21:395502.
[41] Dal Corso A. Pseudopotentials periodic table: from H to Pu. Comput Mater Sci 2014;95:337–50.
[42] Thom PBHES, Gervet FC, Novello WHMMS, Le Provost T, Wallace JSKSM. ECL£ PS® Library Manual. 2000.
[43] Jain A, Ong SP, Hautier G, Chen W, Richards WD, Dacek S, et al. Commentary: the materials project: a materials genome approach to accelerating materials innovation. Appl Mater 2013;1:011002.
[44] Onida G, Reining L, Rubio A. Electronic excitations: density-functional versus many-body Green's-function approaches. Rev Mod Phys 2002;74:601.
[45] Stewart JJ. MOPAC: a semiempirical molecular orbital program. J Comput Aided Mol Des 1990;4:1–103.
[46] Marini A, Hogan C, Grüning M, Varsano D. Yambo: an ab initio tool for excited state calculations. Comput Phys Commun 2009;180:1392–403.
[47] Kang W, Hybertsen MS. Quasiparticle and optical properties of rutile and anatase TiO_2. Phys Rev B 2010;82:085203.
[48] Lucarini V, Saarinen JJ, Peiponen K-E, Vartiainen EM. Kramers-Kronig relations in optical materials research. Springer Science & Business Media; 2005.
[49] Houmad M, Zaari H, Benyoussef A, El Kenz A, Ez-Zahraouy H. Optical conductivity enhancement and band gap opening with silicon doped graphene. Carbon 2015;94:1021–7.
[50] Arbi M, Benramdane N, Kebbab Z, Miloua R, Chiker F, Khenata R. First principles calculations of structural, electronic and optical properties of zinc aluminum oxide. Mater Sci Semicond Process 2012;15:301–7.
[51] Wang B-T, Souvatzis P, Eriksson O, Zhang P. Lattice dynamics and chemical bonding in Sb_2Te_3 from first-principles calculations. J Chem Phys 2015;142:174702.
[52] Stoffel RP, Deringer VL, Simon RE, Hermann RP, Dronskowski R. A density-functional study on the electronic and vibrational properties of layered antimony telluride. J Phys Condens Matter 2015;27:085402.
[53] Souza S, Poffo C, Trichês D, De Lima J, Grandi T, Polian A, et al. High pressure monoclinic phases of Sb_2Te_3. Physica B 2012;407:3781–9.
[54] Anderson TL, Krause HB. Refinement of the Sb_2Te_3 and Sb_2Te_2Se structures and their relationship to nonstoichiometric Sb_2Te_3-ySey compounds. Acta Crystallogr Sect B 1974;30:1307–10.
[55] Jacobsen M, Kumar R, Cornelius A, Nico M, Sinogeiken S. High pressure X-ray diffraction studies of Bi2-xSbxTe3(x = 0, 1, 2). AIP Conference Proceedings 2007.
[56] Li Z, Si C, Zhou J, Xu H, Sun Z. Yttrium-doped Sb_2Te_3: a promising material for phase-change memory. ACS Appl Mater Interfaces 2016;8:26126–34.
[57] Zhang J-M, Ming W, Huang Z, Liu G-B, Kou X, Fan Y, et al. Stability, electronic, and magnetic properties of the magnetically doped topological insulators Bi2Se3, Bi_2Te_3, and Sb_2Te_3. Phys Rev B 2013;88:235131.
[58] Nguyen T-A, Backes D, Singh A, Mansell R, Barnes C, Ritchie DA, et al. Topological states and phase transitions in Sb2Te3GeTe multilayers. arXiv preprint arXiv:160507214. 2016.
[59] Lefebvre I, Lannoo M, Allan G, Ibanez A, Fourcade J, Jumas J, et al. Electronic properties of antimony chalcogenides. Phys Rev Lett 1987;59:2471.

[60] Lu Q, Zhang H-Y, Cheng Y, Chen X-R, Ji G-F. Phase transition, elastic and electronic properties of topological insulator Sb_2Te_3 under pressure: first principle studyProject supported by the National Natural Science Foundation of China (Grant Nos. 11204192 and 11174214) and Jointly supported by the National Natural Science Foundation of China and the China Academy of Engineering Physics (NSAF) (Grant No. U1430117). Chin Phys B 2016;25:026401.

[61] Nakrela A, Benramdane N, Bouzidi A, Kebbab Z, Medles M, Mathieu C. Site location of Al-dopant in ZnO lattice by exploiting the structural and optical characterisation of ZnO: Al thin films. Results Phys 2016;6:133–8.

[62] Penn DR. Wave-number-dependent dielectric function of semiconductors. Phys Rev 1962;128:2093.

[63] Koc H, Ozisik H, Deligöz E, Mamedov AM, Ozbay E. Mechanical, electronic, and optical properties of Bi2S3 and Bi2Se3 compounds: first principle investigations. J Mol Mod 2014;20:1–12.